HHS Public Access

Author manuscript

Clin Cancer Res. Author manuscript; available in PMC 2016 August 15.

Published in final edited form as:

Clin Cancer Res. 2015 August 15; 21(16): 3771–3782. doi:10.1158/1078-0432.CCR-14-3145.

TLR9-Targeted STAT3 Silencing Abrogates Immunosuppressive Activity of Myeloid-Derived Suppressor Cells from Prostate Cancer Patients

Dewan M. S. Hossain[1], **Sumanta K. Pal**[2,6], **Dayson Moreira**[1], **Priyanka Duttagupta**[1], **Qifang Zhang**[1], **Haejung Won**[1], **Jeremy Jones**[3], **Massimo D'Apuzzo**[4], **Stephen Forman**[5], and **Marcin Kortylewski**[1,6]

[1]Departments of Cancer Immunotherapeutics & Tumor Immunology; Beckman Research Institute at City of Hope, Duarte, CA 91010, USA

[2]Medical Oncology and Experimental Therapeutics; Beckman Research Institute at City of Hope, Duarte, CA 91010, USA

[3]Cancer Biology; Beckman Research Institute at City of Hope, Duarte, CA 91010, USA

[4]Department of Pathology; Beckman Research Institute at City of Hope, Duarte, CA 91010, USA

[5]Hematology and Hematopoietic Cell Transplantation; Beckman Research Institute at City of Hope, Duarte, CA 91010, USA

Abstract

Purpose—Recent advances in immunotherapy of advanced human cancers underscored the need to address and eliminate tumor immune evasion. The myeloid-derived suppressor cells (MDSCs) are important inhibitors of T cell responses in solid tumors, such as prostate cancers. However, targeting MDSCs proved challenging due to their phenotypic heterogeneity.

Experimental Design—Myeloid cell populations were evaluated using flow cytometry on blood samples, functional assays and immunohistochemical/immunofluorescent stainings on tumor/tumor-draining lymph node specimens from healthy subjects, localized and metastatic castration-resistant prostate cancer patients.

Results—Here, we identify a population of $Lin^{-}CD15^{HI}CD33^{LO}$ granulocytic MDSCs that accumulate in patients' circulation during prostate cancer progression from localized to metastatic disease. The prostate cancer-associated MDSCs potently inhibit autologous $CD8^{+}$ T cells proliferation and production of IFNγ and Granzyme-B. The circulating MDSCs have high levels of activated STAT3, which is a central immune checkpoint regulator. The granulocytic $pSTAT3^{+}$

[6]Correspondence should be addressed to: Marcin Kortylewski, Ph.D., 1500 East Duarte Rd., Duarte, CA 91010; phone: (626) 256-4673 ext.64120; fax: (626) 471-3602; mkortylewski@coh.org or Sumanta K. Pal, Ph.D., 1500 East Duarte Rd., Duarte, CA 91010; phone: (626) 256-4673 ext.68230; fax: (626) 301-8233; spal@coh.org.

AUTHORSHIP CONTRIBUTIONS

Contribution: D.M.S.H., D.M., P.D., H.W. performed research; D.M.S.H., M.K. designed experiments; D.M.S.H., D.M., J.J., M.D. S.F., S.K.P. and M.K. analyzed the data; D.M.S.H. and M.K. wrote the manuscript.

Conflict-of-interest statement: The authors have declared that no conflict of interest exists.

The authors have no conflicting financial interests.

cells are also detectable in patients' prostate tissues. We previously generated an original strategy to silence genes specifically in Toll-like Receptor-9 (TLR9) positive myeloid cells using CpG-siRNA conjugates. We demonstrate that human granulocytic MDSCs express TLR9 and rapidly internalize naked CpG-*STAT3*siRNA thereby silencing *STAT3* expression. STAT3 blocking abrogates immunosuppressive effects of patients-derived MDSCs on effector $CD8^+$ T cells. These effects depended on reduced expression and enzymatic activity of Arginase-1, a downstream STAT3 target gene and a potent T cell inhibitor.

Conclusions—Overall, we demonstrate the accumulation of granulocytic MDSCs with prostate cancer progression and the feasibility of using TLR9-targeted *STAT3*siRNA delivery strategy to alleviate MDSC-mediated immunosuppression.

Keywords

MDSC; TLR9; STAT3; arginase; prostate cancer

INTRODUCTION

Prostate cancer remains the most common malignancy in men in the United States (1). Although, localized prostate cancers are curable with surgery or standard therapeutic regimens, the five-year survival rate of patients with the advanced metastatic tumors is reduced to 20-30%. Androgen deprivation therapies control the recurrent disease only for limited time until the development of metastatic castration-resistant prostate cancers (mCRPC). Current chemotherapeutic regimens for mCRPC have limited efficacy and are plagued by the highly toxic effects to normal tissues (2). The first FDA-approved immunotherapeutic approach to mCRPC, using autologous cellular vaccinations, showed promising although modest improvement in patients' survival (3). Growing evidence suggests that prostate tumor microenvironment can block immune responses using a wide array of immune checkpoint mechanisms likely extending beyond PD-1 blockade (4-7). Human tumors recruit and expand population of potently immunosuppressive myeloid-derived suppressor cells (MDSCs) which were associated with progression and poor patients' survival (8-10). Depending on the expression of lineage-specific immune markers, MDSCs can be divided into $CD14^+CD15^{LO}CD33^{HI}$ monocytic MDSCs (M-MDSCs) and $CD14^-CD15^{HI}CD33^{LO}$ granulocytic MDSCs (G-MDSCs), also known as polymorphonuclear neutrophil-MDSCs (PMN-MDSC)(8). The generation of MDSCs is a result of tumor-induced skewing of monocyte differentiation from macrophages/DCs into M-MDSCs and later into G-MDSCs, a dominant myeloid population in cancer patients' circulation (11). First study that reported circulating prostate cancer-associated MDSCs in patients with the localized disease identified these cells as $CD14^+$/HLA-DR^- M-MDSCs (12). Whether G-MDSCs are contributing to prostate cancer progression remains unknown. However, there is accumulating evidence linking G-MDSCs with immunosuppression in human genitourinary tumors, such as renal and bladder cancers (13-16). Preclinical studies in mouse tumor models showed that MDSC depletion or targeting their expansion and recruitment increases the effectiveness of cancer therapies, including anti-PD-1 immunotherapies (8, 17). We also recently observed that resistance of renal carcinoma patients to pazopanib, a multi-receptor tyrosine kinase inhibitor and antitangiogenic agent,

correlated with accumulation of $CD15^+$ G-MDSCs in circulation compared to patients responding to therapy (18).

The expansion of MDSCs in the tumor microenvironment is induced by cancer-derived mediators, such as VEGF, HGF, G-CSF, IL-6 and IL-10 (19). Downstream signaling induced by majority of these factors converges on signal transducer and activator of transcription 3 (STAT3), which plays central role in the expansion and function of MDSCs (19, 20). Tumor-induced STAT3 activation in myeloid cells inhibits differentiation while enhancing their survival through upregulation of Bcl-X_L, c-Myc and Cyclin D1 (19, 20). In addition, STAT3 promotes immunosuppressive functions of MDSCs by stimulating expression of Arginase-1, ROS, iNOS and IDO (19, 21). Targeting STAT3 is therefore an attractive strategy to alleviate MDSC-mediated immunosuppression in the tumor microenvironment without the need for myeloid cell depletion. However, as a molecule without enzymatic activity, STAT3 has proven to be a challenging target for pharmacologic inhibition. Small molecule tyrosine kinase inhibitors are an alternative strategy to target STAT3, but therapeutic effects in most clinical trials were short-lived (22).

We previously generated an original method to silence genes specifically in human and mouse $TLR9^+$ myeloid cells using siRNA molecules conjugated to CpG oligonucleotides (23, 24). Targeted TLR9 activation and STAT3 blocking using CpG-*STAT3* siRNA alone, or in combination with radiotherapy, overcame immunosuppression and generated antitumor immune responses against various solid tumors in mice (23, 25). In the present study, we demonstrate that a population of GMDSCs with high levels of STAT3 activity and Arginase-1 expression is associated with progression of prostate cancers from localized to metastatic disease. We also tested the feasibility of using CpG-*STAT3*siRNA to abrogate immunosuppressive functions of prostate cancer-associated G-MDSCs on effector T cell activities. Overall, these studies provide a rational for application of CpG-*STAT3* siRNA strategy to immunotherapy of human prostate cancers.

MATERIALS AND METHODS

Patients

Blood specimens were collected prospectively (after informed consent was obtained) from patients under two independent protocols, IRB-11020 and IRB-10058 (COH). In the IRB-11020, selected patients were diagnosed with high-risk localized prostate cancers. Blood specimens were collected at the baseline before patients underwent prostatectomy. Patients in the IRB-10058 were diagnosed with metastatic castration-resistant prostate cancers (mCRPC) and were later treated with docetaxel chemotherapy. Blood specimens were collected at baseline and after 4 months of docetaxel chemotherapy applied in 3 weekly cycles. Prostatectomy specimens were acquired from patients with high-risk, localized prostate cancers under IRB-10151 protocol (COH). Each protocol and the relevant informed consent were approved by the institutional scientific review committee, data safety monitoring board, and the institutional review board at City of Hope. All patients enrolled provided written informed consent, and the study was conducted in accordance with the amended Declaration of Helsinki and the International Conference on Harmonization Guidelines.

PBMC isolation and flow cytometry

PBMCs and plasma were separated using Vacutainer CPT tubes (BD) within 2 h after collection by centrifugation at 1800×g for 20 min at room temperature. Fresh PBMCs were used for phenotypic analysis of myeloid immune cell populations, 1×10^6 of PBMCs were pre-incubated with FcγIII/IIR-specific antibody to block unspecific binding and then stained with fluorescently-labeled antibodies to HLA-DR, CD11b, CD14, CD3, CD19, CD56, CD114, CD15 or CD33 (eBiosciences). For analysis of intracellular markers, we used PBMCs previously frozen in optimized Cryostor CS5 media (Biolife). Freeze/thaw procedure reduced CD15 staining causing decrease in the percentage of $CD15^{HI}CD33^{LO}$ cells (Supplementary Figure S1), however, reductions of G-MDSC percentages were consistent between various patients. Thus, it was feasible and acceptable to compare identically handled cryopreserved samples to assess relative changes of G-MDSC population during disease progression. For intracellular staining, PBMCs were first stained for surface markers, then fixed and permeabilized using BD fixation and perm/wash buffer, respectively, following manufacturer's recommendations. After blocking in human serum, cells were stained using fluorescently-labeled antibodies specific to TLR9 (eBiosciences), tyrosine 705-phosphorylated STAT3 (pSTAT3; BD Biosciences) or Arginase-1 (R&D systems). Flow cytometric data were collected on BD-Accuri C6 Flow Cytometer (BD) or MACSQuant (Miltenyi Biotec) and analyzed using FlowJo software (Tree Star, Ashland, OR).

MDSC isolation and treatment

For analysis of immunosupressive functions, myeloid cell populations were isolated from fresh blood samples using FACSAriaIII cell sorter (BD-Biosciences) or magnetic enrichment (Stemcell). For the latter, $CD14^+$ cells were first removed from total PBMCs using specific antibodies (eBiosciences) and then $CD14^-CD15^+$ cells were selected using CD15-specific antibodies (eBiosciences). Purity of isolated cells was evaluated by flow cytometry which detected single cell population (data not shown). For the analysis of STAT3 activation and ARG1 expression, frozen PBMCs were thawed and cultured for at least 2 h in 20% plasma from the same patient. These conditions were sufficient to restore the maximum levels of STAT3 signaling as determined in preliminary studies (Supplementary Figure S2). Then selected myeloid cell populations were isolated using high speed cell sorting using FACS-Aria (BD) or magnetic separation using specific antibodies (Stemcell Technologies). For the latter, after removal of $CD14^+$ myeloid cells from total PBMCs using CD14-specific antibodies (eBiosciences), the $CD14^-CD15^+$ cells were enriched from the remaining PBMCs using CD15-specific antibody (eBiosciences). For uptake studies, enriched MDSCs were treated using different concentrations of FITC-labeled CpG-*STAT3* siRNA followed by flow cytometry to assess the uptake. The sequences of human cell-specific CpG-siRNAs were reported before (23, 24). All CpG-siRNA conjugates were synthesized at DNA/RNA Synthesis Core (COH) by using 5 units of C3 carbon chain, (CH2)3 (Glen Research) to link the D19 oligodeoxyribonucleotides to antisense strands (AS) of siRNAs. The resulting constructs were hybridized to complementary siRNA sense strands (SS) to generate CpG-siRNA conjugates. To test the effect of STAT3 or Arginase-1 inhibition on MDSC function, the isolated MDSCs were treated with 500nM of CpG-*STAT3*

siRNA or 20μM nor-NOHA (Cayman Chemical) and then co-cultured with autologous T cells.

T cell assays

$CD3^+$ T cells were isolated from patients' PBMCs using specific antibodies plus magnetic bead-enrichment (Stemcell Technologies) and then labeled using carboxyfluorescein succinimidyl ester (CFSE; Life Technologies). CFSE-labeled cells were then incubated with Human T cell Activator CD3/CD28 Dynabeads (Life Technologies) for 3 days with or without $CD15^{HI}CD33^{LO}$ MDSCs isolated from same patient. Proliferation of $CD3^+$ T cells were evaluated as CFSE dilution using flow cytometry. To determine IFNγ and granzyme-B response in $CD8^+$ T cells in same experimental condition, Golgi stop (BD biosciences) was added for last 6 h to the MDSC-T cell co-cultures and harvested cells were immunostained with specific antibodies to CD3, CD8, IFNγ and granzyme-B (BD) according to manufacturer's protocol. Unstimulated $CD3^+$ T cells from each patient served as a negative control.

Quantitative real-time PCR and protein assays

For quantitative PCR (qPCR), total RNA was extracted from isolated MDSCs using the RNeasy Plus kit (QIAGEN). After cDNA synthesis using iScript kit (Bio-Rad), samples were analyzed using sets of probes from the Universal Probe Library and specific primer pairs for human *STAT3*: 5′-CTGCCTAGATCGGCTAGAAAAC-3′, 5′-CCCTTTGTAGGAAACTTTTTGC-3′, UPL #25; *TLR9*: 5′-TGTGAAGCATCCTTCCCTGTA-3′, 5′-GAGAGACAGCGGGTGCAG-3′, UPL #56. SsoAdvanced SYBER Green super mix (Bio-Rad) was used to analyze human *ARG-1*, *iNOS and IDO* expression in patient MDSCs with following sets of primers: *ARG-1*: 5'-GTTTCTCAAGCAGACCAGCC-3' and 5'-GCTCAAGTGCAGCAAAGAGA-3'; *iNOS*: 5'-ATTCTGCTGCTTGCTGAGGT-3' and 5'-TTCAAGACCAAATTCCACCAG-3'; *IDO:* 5'-CATCTGCAAATCGTGACTAAG-3' and 5'-CAGTCGACACATTAACCTTCCTTC-3'. Sequence-specific amplification was analyzed on the CFX96 Real-Time PCR Detection System (Bio-Rad). The data were normalized to the *TBP* expression and the relative expression levels were calculated using the $2^{-\Delta\Delta Ct}$ method. Concentrations of cytokines and growth factors were assessed in plasma specimens using Human Cytokine 30-plex protein assay (Invitrogen) on FLEXMAP 3D System (Luminex) at the Clinical Immunobiology and Correlative Studies Laboratory (City of Hope).

Arginase activity assay

Arginase-1 enzymatic activity in $CD15^{HI}CD33^{LO}$ cell lysates and blood serum from different stage prostate cancer patients were measured using QuantiChrom™ Arginase Assay Kit (BioAssay Systems). To prepare lysates, isolated MDSCs were lysed with 10 mM Tris-HCL (pH 7.4) containing protease inhibitors (Complete Mini, Roche) and 0.4% Triton X-100 for 15 min on ice. For blood serum samples, urea was removed using Amicon Ultra-0.5 centrifugal filter devices (Millipore).

Immunohistochemistry and confocal microscopy

For immunohistochemical analysis, 4 μm sections were deparaffinized and immunostained using antibodies specific for CD15 (Abcam) or pSTAT3 (Cell Signaling). The slides were analyzed first using upright AX70 microscope (Olympus) followed by whole slide imaging using NanoZoomer scanner and NDP v.2.5 software (Hamamatsu Photonics). To assess the morphology of $CD15^{HI}CD33^{LO}$ and $CD15^{LO}CD33^{HI}$ populations, sorted cells were cytospinned on glass slides and dried for 10 min at room temperature. Slides were then vertically submersed in methanol for 15 min, stained briefly using Differential Quick Stain kit (Polyscienecs, Inc), coverslipped with mounting medium (Vector Labs) and imaged using upright AX70 microscope (Olympus). For *in vitro* uptake studies, $CD15^{+}CD14^{-}$ cells enriched from prostate cancer patient were incubated with fluorescently labeled CpG-*STAT3*$siRNA^{FITC}$ (500 nM) for various times. Cell were then fixed using 1.6% paraformadehyde, permeabilized using 0.5% Triton/PBS and washed. After a cytospin onto the poly-L-lysine (Sigma-Aldrich) coated slides, cells were mounted in Vectashield Hard-set mounting medium with DAPI (Vector Laboratories) for confocal microscopy. The confocal imaging was carried out using a 63x oil immersion objective on LSM-510 Meta inverted confocal microscope (Zeiss).

Statistical Analysis

Unpaired *t* test was used to calculate the two-tailed *P* value to estimate statistical significance of differences between two experimental groups. One- or two-way ANOVA plus Bonferroni posttest were applied to assess the statistical significance of differences between multiple treatment groups or patients from different stages and healthy donors. Statistically significant *P* values are indicated in the figures with asterisks: ***$P < 0.001$; **$P < 0.01$; *$P < 0.05$. Data were analyzed using Prism v.6.0 software (GraphPad).

RESULTS

Prostate cancer progression is associated with the accumulation of circulating $CD15^{HI}CD33^{LO}$ granulocytic myeloid cells

We used flow cytometry to phenotype immune cell populations in blood derived from patients with localized or metastatic prostate cancers compared to healthy subjects. As shown in Figure 1AB, increased percentages of circulating myeloid cell subsets were more sensitive indicators of tumor presence and progression than changes in lymphoid cell populations, such as regulatory T cells, or in plasmacytoid DCs (Supplementary Figure S3). Compared to controls both groups of prostate cancer patients showed significant accumulation of blood $CD15^{HI}CD33^{LO}$ granulocytic myeloid cells while the percentage of $CD15^{LO}CD33^{HI}$ myeloid cells did not change (Figure 1B). In addition, the percentage of $CD15^{HI}CD33^{LO}$ granulocytic myeloid cells was increased more than twice in mCRPC patients compared to patients with localized tumors (Figure 1B). The percentage of $CD15^{HI}CD33^{LO}$ myeloid cells in mCRPC patients remained elevated even after standard docetaxel treatment regimen (Supplementary Figure S4). Further phenotypic characterization indicated that both myeloid cell populations share expression of the common myeloid marker CD11b while being negative for lineage-markers CD3, CD19 and CD56 (Figure 1C). However, monocytic-lineage marker CD14 and HLA-DR molecules

were expressed only by $CD15^{LO}CD33^{HI}$ and not by $CD15^{HI}CD33^{LO}$ (Figure 1C). Therefore, $CD15^{HI}CD33^{LO}$ cells resemble the granulocytic subtype of myeloid derived suppressor cells (MDSCs) as also indicated by G-CSFR/CD114 expression, which is associated with this subpopulation (Figure 1C)(26). To verify this observation, we next analyzed cytomorphology of both populations after cell sorting. As expected, $CD15^{HI}CD33^{LO}$ cells show polymorphonuclear (PMN) morphology typical for granulocytic cells (upper panel) compared to mononuclear $CD15^{LO}CD33^{HI}$ cells (lower panel) (Figure 1D). The PMN features of $CD15^{+}$ cells, such as partly segmented nuclei, were also detectable in immunohistochemical stainings of prostatectomy sections derived from mCRPC patients (Figure 1E). However, flow cytometric results detected only a small fraction of mature $CD16^{HI}$ neutrophils within $CD15^{HI}CD33^{LO}$ cell compartment which indicates that majority of these cells are immature granulocytes (Figure 1F). Other studies demonstrated the involvement of various cytokines and growth factors in stimulating MDSC expansion (G-CSF, HGF, bFGF), recruitment (IL-8) or differentiation (IFNα)(19). Our further comparative analysis of plasma samples from patients with localized vs. metastatic tumors indicated correlation between the elevated numbers of $CD15^{HI}CD33^{LO}$ cells and the increase in plasma concentrations of G-CSF, HGF, bFGF and IL-8 with the concomitant reduction of proinflammatory IFNα (Figure 1G). Overall, prostate cancer progression from localized to metastatic disease correlates with changes of cytokine/growth factor environment that may promote accumulation of circulating $CD15^{HI}CD33^{LO}$ granulocytic cells.

Granulocytic-MDSCs (G-MDSCs) inhibit proliferation and activity of autologous T cells

We next verified whether prostate cancer-associated $CD15^{+}$ granulocytic cells show immunosuppressive activity. The effect on the proliferation and activities of autologous T cells was assessed using $CD14^{-}$ $CD15^{+}$ cells enriched from mCRPC patients. The $CD14^{+}CD15^{-}$ monocytes were used as a negative control. As shown in Figure 2A-B, the $CD14^{-}CD15^{+}$ myeloid cells reduced CD3/CD28-driven T cell proliferation to ~50% at 2:1 or ~80% at 1:1 ratio of T cells to myeloid cells, respectively. In contrast, the presence of $CD14^{+}CD15^{-}$ monocytes did not significantly alter T cell proliferation. The $CD14^{-}$ $CD15^{+}$ myeloid cells had similar effect on both autologous $CD8^{+}$ and $CD4^{+}$ T cells (Figure 2C) as well as on allogeneic T cells (Supplementary Fig. S5). The $CD14^{-}CD15^{+}$ myeloid cells but not monocytes from mCRPC patients, also strongly inhibited IFNγ (Figure 2D) and granzyme B production by effector $CD8^{+}$ T cells (Figure 2E). These results confirmed that $CD15^{+}$ myeloid cells accumulating in the circulation of prostate cancer patients are functionally MDSCs.

G-MDSCs in circulation show higher level of pSTAT3

Recent clinical studies suggested that STAT3 contributes not only to MDSC expansion, as suggested by mouse tumor models, but plays a critical role for the expression of several mediators of immunosuppression (21, 27). Thus, we used flow cytometry to assess levels of activated and tyrosine-phosphorylated STAT3 (pSTAT3) in G-MDSCs during prostate cancer progression. As shown in Figure 3A, $CD15^{HI}CD33^{LO}$ cells from patients with both localized and metastatic disease had elevated levels of intracellular pSTAT3 compared to control healthy subjects. These changes reflected increase STAT3 activation rather than

upregulated expression of STAT3 total protein, which did not change between healthy subjects and prostate cancer patients (Figure 3B). Importantly, the percentage of G-MDSCs with high STAT3 activity increased significantly during disease progression, reaching maximum in mCRPC patients (Figure 3C). Next, we verified whether $pSTAT3^+$ granulocytic cells are present not only in circulation but also in the prostate cancer microenvironment. Sections of prostatectomy-derived tumors (n = 10) were stained using immunohistochemistry for pSTAT3, counterstained and microscopically analyzed. $pSTAT3^+$ cells with PMN morphology were present in patients' samples and could be found in prostate tissues including lumen of benign glands (Figure 3D). Thus, we conclude that granulocytic $CD15^+/pSTAT3^+$ cells are commonly present in mCRPC patients' circulation and likely reach into the prostate tumor microenvironment.

Prostate cancer-associated G-MDSCs secrete high levels of Arginase-1 (ARG1)

To assess whether G-MDSCs actively contribute to prostate cancer-associated immune evasion, we compared *iNOS*, *IDO* or *ARG1* mRNA levels in $CD15^+/pSTAT3^+$ G-MDSCs sorted from cancer patients in comparison to $CD15^+/pSTAT3^-$ cells in healthy control subjects. The qPCR analysis indicated over 100-fold increase in *ARG1* levels in cancer patients' samples (Figure 4A). In contrast, the *IDO* mRNA increased only 5-fold while there was no effect on *iNOS* expression in the same group of samples. These results were further corroborated by measuring ARG1 enzymatic activity directly in cellular lysates prepared from $CD15^+CD14^-$ cells derived from metastatic prostate cancer patients vs. healthy subjects. $CD15^+CD14^-$ cells from mCRPC patients showed about ten-fold increase in ARG1 activity compared to controls (Figure 4B). In addition, the overall frequency of ARG1 expressing $CD15^{HI}CD33^{LO}$ G-MDSCs increased with progression of the disease (Figure 4C) corresponding to the increase in the percentage of $CD15^+pSTAT3^+$ cells (Figure 3C). At the same time, the intracellular levels of ARG1 protein were comparably high in G-MDSCs from patients with both localized and metastatic prostate cancers (Figure 4D). These changes were paralleled by significantly elevated enzymatic activity of ARG1 in patients' plasma samples during disease progression. Compared to baseline levels in healthy controls, the ARG1 activity was doubled or tripled in patients with localized or metastatic tumors, respectively (Figure 4E). Overall, these data implicate the role of ARG1 in promoting and sustaining the immunosuppressive microenvironment in human prostate cancers.

Prostate cancer-associated G-MDSCs express TLR9 and are effectively targeted by CpG-*STAT3*siRNA conjugates

We previously demonstrated that ligands for the intracellular TLR9 receptor can deliver siRNA molecules into mouse and human target cells (23, 24). The unformulated CpG-siRNA conjugates silence specific genes both *in vitro* and *in vivo*. As verified using real-time qPCR, $CD15^{HI}CD33^{LO}$ G-MDSCs isolated from prostate cancer patients' blood express TLR9 at both mRNA and protein levels similar to B cells used as a positive control (Figure 5A)(24). Next, we determined whether G-MDSCs can internalize CpG-*STAT3*siRNA. PBMCs from late stage prostate cancer patients were incubated for various times and doses with fluorescently labeled CpG-$siRNA^{Cy3}$ or unconjugated $siRNA^{Cy3}$ without any transfection reagents. Already after 30 min. incubation, the uptake of CpG-

*STAT3*siRNA exceeded 80% of G-MDSCs and continued to increase with longer incubation times (Figure 5B, left two panels). At 4 h, the CpG-*STAT3*siRNA was internalized by the majority of cells already at the lowest 100 nM concentration (Figure 5B, middle). In contrast, the G-MDSCs did not internalize the unconjugated *STAT3*siRNA even after 4 h incubation at 500 nM (Figure 5B, right). Confocal microscopy studies showed perinuclear/cytoplasmic localization of the siRNA part of the molecule after uptake by target G-MDSCs (Figure 5C). This is consistent with the TLR9-mediated mechanism of endosomal release of processed CpG-siRNA conjugates (23). Finally, we examined whether CpG-*STAT3*siRNA treatment will result in target gene silencing in G-MDSCs. Magnetically enriched G-MDSCs were incubated for 48 h with 500 nM CpG-siRNA conjugates targeting *STAT3* or *luciferase* genes, the latter being used as a negative, non-targeting control. Both *STAT3* expression and pSTAT3 levels were assessed using qPCR and flow cytometry together with western blotting. CpG-*STAT3* siRNA treatment reduced *STAT3* mRNA expression by ~70% (Figure 5D) and as a result also STAT3 phosphorylation and total protein levels (Figure 5E). Importantly, STAT3 inhibition did not affect G-MDSC viability as verified by flow cytometry (Supplementary Figure S6). Next, we determined the effect of CpG-*STAT3*siRNA on immunosuppressive functions of G-MDSCs. The isolated $CD15^{+}CD14^{-}$ cells were pre-treated using CpG-*STAT3* siRNA or control CpG-*Luc* siRNA overnight and then co-cultured with autologous $CD3^{+}$ T cells (1:1 ratio) with CD3/CD28 costimulation for additional 72 h. As shown in Figure 5F, CpG-*STAT3* siRNA alleviated most of the GMDSC-mediated effect on T cell proliferation. Under the same experimental conditions, we analyzed IFNγ and granzyme B production by $CD8^{+}$ T cells. Both IFNγ (Figure 5G) and granzyme B (Figure 5H) expression levels were restored to ~70% and ~80% of control levels, respectively, after STAT3 blocking in G-MDSCs using CpG-*STAT3*siRNA. Overall, these results suggest the feasibility of using CpG-*STAT3*siRNA strategy for functional depletion of prostate cancer-associated MDSCs.

CpG-*STAT3*siRNA blocks ARG1 production and impairs G-MDSC activity

To gain insights into the mechanism(s) of G-MDSCs loss of function, we assessed the effect of STAT3 inhibition on ARG1 expression. $CD15^{+}CD14^{-}$ cells were isolated from late stage prostate cancer PBMCs and cultured for 48 h in the presence of 500 nM CpG-*STAT3*siRNA or CpG-*Luc*siRNA. As assessed using flow cytometric and colorimetric assays, both ARG1 expression (Figure 6A) and enzymatic activity (Figure 6B) were reduced by ~60% in G-MDSCs following *STAT3* silencing. To verify whether ARG1 actually contributes to STAT3-mediated suppression of T cell activity by G-MDSCs, we repeated T cell proliferation assays using specific inhibitor of arginase activity (nor-NOHA)(21). Prostate cancer-derived G-MDSCs ($CD15^{+}CD14^{-}$) were pre-treated with nor-NOHA alone, CpG-*STAT3* siRNA alone or both reagents combined and then co-cultured with autologous T cells with CD3/CD28-mediated stimulation (Figure 6C). As expected, G-MDSCs treated with nor-NOHA used as a single agent reduced by about half the immunosuppressive effect of G-MDSCs on T cell proliferation (Figure 6D). However, STAT3 blocking using CpG-siRNA alone eliminated most of the G-MDSC effect while the combination with nor-NOHA didn't improve this effect any further (Figure 6D). Overall, these studies provide a proof-of-principle for targeting immunosuppressive STAT3/ARG1 signaling axis in GMDSCs as a

potential therapeutic strategy to disrupt the immunosuppressive microenvironment in prostate cancers.

DISCUSSION

Here, we provide the first evidence of $TLR9^+$ granulocytic MDSCs that accumulate in prostate cancer patients in correlation with disease progression. We also document that these prostate cancer-associated G-MDSCs require high levels of immunosuppressive STAT3 signaling and Arginase-1 activity protein for suppressing effector T cell activity. While our results are based on limited number of patients, pSTAT3-positive granulocytic cells were consistently found not only in blood but also patients' prostatectomy specimens. Finally, we suggest therapeutic strategy for the functional elimination of G-MDSCs using CpG oligonucleotide-mediated delivery of *STAT3* siRNA into these $TLR9^+$ myeloid cells. Overall, our findings indicate new and potentially safer therapeutic approach to mitigate immunosuppression in prostate cancer patients using gene- and cell type-specific inhibitory oligonucleotides.

The relevance of these results for human cancer therapy is underscored by the lack of clinically relevant strategies for eliminating MDSC-dependent immune evasion. In contrast to results of preclinical studies in mice(28), with notable exception of sunitinib effect in renal cancer patients, current cancer therapies usually fail to reduce the elevated levels of MDSCs (Supplementary Figure S4)(8, 15, 18). The G-MDSCs were found in circulation of patients with other genitourinary malignancies, such as renal and bladder cancers and several different solid tumors (11, 13, 15, 16). However, due to complex pattern of surface molecules, partly overlapping with other immune cell lineages, targeting MDSCs through antibody-mediated depletion is challenging. Successful targeting of MDSCs requires identification of functional markers associated with the tumor microenvironment, as shown by promising preclinical results on targeting CXCR2-mediated MDSC tumor trafficking (17). Our findings suggest that intracellular signaling mediators of immunosuppression may provide alternative and even more precise functional MDSC biomarkers. This is of importance given the difficulty in identifying MDSCs among other immune cell populations using surface markers or nuclear morphology, as in case of discerning G-MDSCs from mature neutrophils (29, 30). Thus, the contribution of mature neutrophils to the overall immunosuppressive effect cannot be excluded (29). The constitutive activation of STAT3, a known master regulator of immunosuppression, was lately reported in MDSCs associated with several types of human cancers, such as melanoma, head and neck, renal, breast and pancreatic cancers (15, 21, 27, 31-33). Correspondingly, we have found that majority of granulocytic cells that were infiltrating prostate tissues showed activation of STAT3. These observations merit further studies in a larger set of specimens to validate whether the presence of $CD15^+/pSTAT3^+$ and/or $CD15^+/ARG1^+$ cells can serve as an indicator of the G-MDSC-induced immunosuppressive microenvironment in prostate cancers. It is known that immunosuppressive activity of G-MDSCs depends mainly on Arginase-1 expression rather than iNOS activity for their function (19). This is consistent with our data from patients' G-MDSCs, in comparison to normal granulocytic cells, that showed highly elevated levels of *ARG1*, weak induction of *IDO* and no detectable effect on *iNOS* expression. These results seem to reflect different level of STAT3 involvement in the regulation of these target genes.

In MDSCs, STAT3 was shown to have potent and direct effect on *ARG1*, while it collaborates with noncanonical NF-κB signaling to promote *IDO* expression (19, 21, 32). In contrast, STAT3 activity is not required for *iNOS* expression which is driven by STAT1 and NF-κB signaling activated in monocytic MDSCs but not in G-MDSCs (19).

TLR9 was recently found to be expressed by tumor-associated MDSCs in mice, with its highest levels observed in M-MDSCs (34, 35). This is consistent with the common expression of TLR9 in mouse myeloid cells (36). Although TLR9 expression in humans is more restricted than in mice, recent studies reported that environmental factors such as GM-CSF can induce TLR9 in differentiating monocytes and neutrophils (24, 37, 38). TLR9 expression in prostate cancer patients' G-MDSCs is likely associated with the multiple soluble factors released from the tumor microenvironment (Figure 1G). Downstream TLR9 signaling through MyD88 and NF-κB contributes to myeloid cell-driven inflammatory responses in reaction to tissue stress and injury (39-41). Interestingly, two reports showed that intratumoral injections of high doses of synthetic TLR9 agonists, CpG oligodeoxynucleotides (ODN), can trigger MDSC differentiation and reduce their immunosuppressive potential in mice (34, 35). These effects were suggested to be either direct or mediated through activation of plasmacytoid DCs and production of type I IFNs. However, numerous clinical trials using CpG ODNs proved that generation of systemic antitumor immune responses is challenging due to immunosuppressive effects of the tumor microenvironment (42). Other studies in mouse tumor models showed that activation of TLRs in myeloid cells can in fact promote expression of immunosuppressive molecules critical for MDSC function, such as Arginase-1, S100A8, IL-10 and PGE_2 (19, 43-45). The functional dichotomy of TLR9 effects results from crosstalk with other signaling pathways operating under normal or tumor-induced inflammatory conditions. The outcome of TLR9 signaling seems to be defined by a multilayered negative feedback regulation through STAT3 (41, 46). Our own studies in mouse solid tumor models revealed that pre-existing STAT3 activity in tumor-associated myeloid cells, such as macrophages and MDSCs, can skew TLR9 signaling towards supporting tumor angiogenesis while blocking antitumor immunity (25, 46). Whether TLR9 contributes to immunosuppressive potential of prostate cancer-associated MDSCs remains to be established in more extensive molecular studies.

STAT3 provides an attractive therapeutic target in tumor-associated myeloid cells (20, 41). At the same time, the role of STAT3 signaling in T lymphocytes is complex. While STAT3 reduces antitumor activity of effector CD8 T cells and promotes generation of tumor-promoting Th17 cells, it is also necessary for the generation of memory T cells and prolonged antitumor immune responses (47-49). Thus, targeting STAT3 for cancer immunotherapy requires myeloid cell-specific strategies to avoid unpredictable adverse effects and toxicities. For example, recent study in mouse melanoma models demonstrated that small molecule drug targeting upstream STAT3 activators, JAK1/2 kinases, reduced numbers of MDSCs while increasing their immunosuppressive potential and blocking T cell proliferation (50). We previously demonstrated that TLR9 agonists, CpG ODN, can be utilized for delivery of therapeutic siRNA molecules into $TLR9^+$ cells in both mouse and human systems (23, 24). Targeting STAT3 with parallel TLR9 activation using CpG-*STAT3*siRNA was shown to eliminate tumorigenic effects of TLR signaling in mouse tumor

models (25). Here, we demonstrated that CpG-siRNA strategy allows for targeting of TLR9$^+$ G-MDSCs to eliminate their immunosuppressive functions without myeloid cell depletion. Further studies should determine whether CpG-*STAT3*siRNA only modulates G-MDSC activity or induces their differentiation into mature granulocytes or DCs/macrophages. Correspondingly, we previously observed that CpG-STAT3siRNA induces activity of neutrophils against blood cancer xenotransplants in NSG mice (24). Independently from this manuscript, we recently identified that prostate cancer propagating cells in human tumors express TLR9 and it is feasible to target this cancer cell population using CpG-siRNA approach (Moreira and Kortylewski; unpublished results). Taken together, our findings provide support for application of CpG-*STAT3*siRNA strategy to immunotherapy of advanced prostate cancers alone or in combination with immunotherapies, such as Sipuleucel-T treatment or emerging T cell-based therapies. Disruption of STAT3 signaling in the tumor microenvironment with concurrent TLR9 stimulation has potential to disrupt the central immunosuppressive circuit paving way to effective antitumor immune responses without toxicities associated with pharmacological agents.

Supplementary Material

Refer to Web version on PubMed Central for supplementary material.

ACKNOWLEDGEMENTS

We would like to thank Dr. Robert Hickey (Translational Biomarker Discovery Core) and acknowledge the dedication of staff members at the Analytical Cytometry, Microscopy, Pathology Core Facilities, Animal Resource Center and at COH. This work was supported in part by the National Cancer Institute of the National Institutes of Health award number R01CA155367, the Department of Defence grant W81XWH-12-1-0132, the Movember-Prostate Cancer Foundation Award, STOP CANCER Foundation Allison Tovo-Dwyer Memorial Career Development Award (to M.K.) and by the National Cancer Institute Grant P30 CA033572 (to COH). The content is solely the responsibility of the authors and does not necessarily represent the official views of the National Institutes of Health.

REFERENCES

1. Jemal A, Siegel R, Xu J, Ward E. Cancer statistics, 2010. CA: a cancer journal for clinicians. 2010; 60:277–300. [PubMed: 20610543]
2. de Bono JS, Oudard S, Ozguroglu M, Hansen S, Machiels JP, Kocak I, et al. Prednisone plus cabazitaxel or mitoxantrone for metastatic castration-resistant prostate cancer progressing after docetaxel treatment: a randomised open-label trial. Lancet. 2010; 376:1147–54. [PubMed: 20888992]
3. Kantoff PW, Higano CS, Shore ND, Berger ER, Small EJ, Penson DF, et al. Sipuleucel-T immunotherapy for castration-resistant prostate cancer. N Engl J Med. 2010; 363:411–22. [PubMed: 20818862]
4. Whiteside TL. Inhibiting the inhibitors: evaluating agents targeting cancer immunosuppression. Expert opinion on biological therapy. 2010; 10:1019–35. [PubMed: 20415597]
5. May KF Jr. Gulley JL, Drake CG, Dranoff G, Kantoff PW. Prostate Cancer Immunotherapy. Clin Cancer Res. 2011; 17:5233–38. [PubMed: 21700764]
6. Sottnik JL, Zhang J, Macoska JA, Keller ET. The PCa Tumor Microenvironment. Cancer Microenviron. 2011; 3:283–97. [PubMed: 21728070]
7. Topalian SL, Hodi FS, Brahmer JR, Gettinger SN, Smith DC, McDermott DF, et al. Safety, activity, and immune correlates of anti-PD-1 antibody in cancer. N Engl J Med. 2012; 366:2443–54. [PubMed: 22658127]

8. Gabrilovich DI, Ostrand-Rosenberg S, Bronte V. Coordinated regulation of myeloid cells by tumours. Nat Rev Immunol. 2012; 12:253–68. [PubMed: 22437938]
9. Diaz-Montero CM, Salem ML, Nishimura MI, Garrett-Mayer E, Cole DJ, Montero AJ. Increased circulating myeloid-derived suppressor cells correlate with clinical cancer stage, metastatic tumor burden, and doxorubicin-cyclophosphamide chemotherapy. Cancer Immunol Immunother. 2009; 58:49–59. [PubMed: 18446337]
10. Greten TF, Manns MP, Korangy F. Myeloid derived suppressor cells in human diseases. International immunopharmacology. 2011; 11:802–7. [PubMed: 21237299]
11. Youn JI, Kumar V, Collazo M, Nefedova Y, Condamine T, Cheng P, et al. Epigenetic silencing of retinoblastoma gene regulates pathologic differentiation of myeloid cells in cancer. Nat Immunol. 2013; 14:211–20. [PubMed: 23354483]
12. Vuk-Pavlovic S, Bulur PA, Lin Y, Qin R, Szumlanski CL, Zhao X, et al. Immunosuppressive CD14+HLA-DRlow/- monocytes in prostate cancer. Prostate. 2009; 70:443–55. [PubMed: 19902470]
13. Kusmartsev S, Su Z, Heiser A, Dannull J, Eruslanov E, Kubler H, et al. Reversal of myeloid cell-mediated immunosuppression in patients with metastatic renal cell carcinoma. Clin Cancer Res. 2008; 14:8270–8. [PubMed: 19088044]
14. Rodriguez PC, Ernstoff MS, Hernandez C, Atkins M, Zabaleta J, Sierra R, et al. Arginase I-producing myeloid-derived suppressor cells in renal cell carcinoma are a subpopulation of activated granulocytes. Cancer Res. 2009; 69:1553–60. [PubMed: 19201693]
15. Ko JS, Zea AH, Rini BI, Ireland JL, Elson P, Cohen P, et al. Sunitinib mediates reversal of myeloid-derived suppressor cell accumulation in renal cell carcinoma patients. Clin Cancer Res. 2009; 15:2148–57. [PubMed: 19276286]
16. Eruslanov E, Neuberger M, Daurkin I, Perrin GQ, Algood C, Dahm P, et al. Circulating and tumor-infiltrating myeloid cell subsets in patients with bladder cancer. Int J Cancer. 2012; 130:1109–19. [PubMed: 21480223]
17. Highfill SL, Cui Y, Giles AJ, Smith JP, Zhang H, Morse E, et al. Disruption of CXCR2-mediated MDSC tumor trafficking enhances anti-PD1 efficacy. Science translational medicine. 2014; 6:237ra67.
18. Pal SK, Sakib Hossain DM, Zhang Q, Frankel PH, Jones JO, Carmichael C, et al. Pazopanib as third-line therapy for metastatic renal cell carcinoma: Clinical efficacy and temporal analysis of cytokine profile. The Journal of urology. 2014; 14:4591–1.
19. Gabrilovich DI, Nagaraj S. Myeloid-derived suppressor cells as regulators of the immune system. Nat Rev Immunol. 2009; 9:162–74. [PubMed: 19197294]
20. Yu H, Kortylewski M, Pardoll D. Crosstalk between cancer and immune cells: role of STAT3 in the tumour microenvironment. Nat Rev Immunol. 2007; 7:41–51. [PubMed: 17186030]
21. Vasquez-Dunddel D, Pan F, Zeng Q, Gorbounov M, Albesiano E, Fu J, et al. STAT3 regulates arginase-I in myeloid-derived suppressor cells from cancer patients. J Clin Invest. 2013; 123:1580–9. [PubMed: 23454751]
22. Wesolowski R, Markowitz J, Carson WE 3rd. Myeloid derived suppressor cells - a new therapeutic target in the treatment of cancer. Journal for Immunotherapy of Cancer. 2013; 1:10. [PubMed: 24829747]
23. Kortylewski M, Swiderski P, Herrmann A, Wang L, Kowolik C, Kujawski M, et al. In vivo delivery of siRNA to immune cells by conjugation to a TLR9 agonist enhances antitumor immune responses. Nat Biotechnol. 2009; 27:925–32. [PubMed: 19749770]
24. Zhang Q, Hossain DM, Nechaev S, Kozlowska A, Zhang W, Liu Y, et al. TLR9-mediated siRNA delivery for targeting of normal and malignant human hematopoietic cells in vivo. Blood. 2013; 121:1304–15. [PubMed: 23287859]
25. Gao C, Kozlowska A, Nechaev S, Li H, Zhang Q, Hossain DM, et al. TLR9 Signaling in the Tumor Microenvironment Initiates Cancer Recurrence after Radiotherapy. Cancer Res. 2013; 73:7211–21. [PubMed: 24154870]
26. Waight JD, Hu Q, Miller A, Liu S, Abrams SI. Tumor-derived G-CSF facilitates neoplastic growth through a granulocytic myeloid-derived suppressor cell-dependent mechanism. PloS one. 2011; 6:e27690. [PubMed: 22110722]

27. Poschke I, Mougiakakos D, Hansson J, Masucci GV, Kiessling R. Immature immunosuppressive CD14+HLA-DR-/low cells in melanoma patients are Stat3hi and overexpress CD80, CD83, and DC-sign. Cancer Res. 2010; 70:4335–45. [PubMed: 20484028]
28. Kodumudi KN, Woan K, Gilvary DL, Sahakian E, Wei S, Djeu JY. A novel chemoimmunomodulating property of docetaxel: suppression of myeloid-derived suppressor cells in tumor bearers. Clin Cancer Res. 2010; 16:4583–94. [PubMed: 20702612]
29. Brandau S, Moses K, Lang S. The kinship of neutrophils and granulocytic myeloid-derived suppressor cells in cancer: cousins, siblings or twins? Semin Cancer Biol. 2013; 23:171–82. [PubMed: 23459190]
30. Pillay J, Kamp VM, van Hoffen E, Visser T, Tak T, Lammers JW, et al. A subset of neutrophils in human systemic inflammation inhibits T cell responses through Mac-1. J Clin Invest. 2012; 122:327–36. [PubMed: 22156198]
31. Mace TA, Ameen Z, Collins A, Wojcik S, Mair M, Young GS, et al. Pancreatic cancer-associated stellate cells promote differentiation of myeloid-derived suppressor cells in a STAT3-dependent manner. Cancer Res. 2013; 73:3007–18. [PubMed: 23514705]
32. Yu J, Wang Y, Yan F, Zhang P, Li H, Zhao H, et al. Noncanonical NF-kappaB activation mediates STAT3-stimulated IDO upregulation in myeloid-derived suppressor cells in breast cancer. J Immunol. 2014; 193:2574–86. [PubMed: 25063873]
33. Waight JD, Netherby C, Hensen ML, Miller A, Hu Q, Liu S, et al. Myeloid-derived suppressor cell development is regulated by a STAT/IRF-8 axis. J Clin Invest. 2013; 123:4464–78. [PubMed: 24091328]
34. Zoglmeier C, Bauer H, Norenberg D, Wedekind G, Bittner P, Sandholzer N, et al. CpG blocks immunosuppression by myeloid-derived suppressor cells in tumor-bearing mice. Clin Cancer Res. 2011; 17:1765–75. [PubMed: 21233400]
35. Shirota Y, Shirota H, Klinman DM. Intratumoral injection of CpG oligonucleotides induces the differentiation and reduces the immunosuppressive activity of myeloid-derived suppressor cells. J Immunol. 2012; 188:1592–9. [PubMed: 22231700]
36. Hemmi H, Takeuchi O, Kawai T, Kaisho T, Sato S, Sanjo H, et al. A Toll-like receptor recognizes bacterial DNA. Nature. 2000; 408:740–5. [PubMed: 11130078]
37. Hayashi F, Means TK, Luster AD. Toll-like receptors stimulate human neutrophil function. Blood. 2003; 102:2660–9. [PubMed: 12829592]
38. Hoene V, Peiser M, Wanner R. Human monocyte-derived dendritic cells express TLR9 and react directly to the CpG-A oligonucleotide D19. J Leukoc Biol. 2006; 80:1328–36. [PubMed: 17000899]
39. Trinchieri G, Sher A. Cooperation of Toll-like receptor signals in innate immune defence. Nat Rev Immunol. 2007; 7:179–90. [PubMed: 17318230]
40. Kawai T, Akira S. The role of pattern-recognition receptors in innate immunity: update on Toll-like receptors. Nat Immunol. 2010; 11:373–84. [PubMed: 20404851]
41. Murray PJ, Smale ST. Restraint of inflammatory signaling by interdependent strata of negative regulatory pathways. Nat Immunol. 2012; 13:916–24. [PubMed: 22990889]
42. Krieg AM. CpG still rocks! Update on an accidental drug. Nucleic acid therapeutics. 2012; 22:77–89. [PubMed: 22352814]
43. El Kasmi KC, Qualls JE, Pesce JT, Smith AM, Thompson RW, Henao-Tamayo M, et al. Toll-like receptor-induced arginase 1 in macrophages thwarts effective immunity against intracellular pathogens. Nat Immunol. 2008; 9:1399–406. [PubMed: 18978793]
44. Parker KH, Sinha P, Horn LA, Clements VK, Yang H, Li J, et al. HMGB1 Enhances Immune Suppression by Facilitating the Differentiation and Suppressive Activity of Myeloid-Derived Suppressor Cells. Cancer Res. 2014; 74:5723–33. [PubMed: 25164013]
45. Hsu K, Chung YM, Endoh Y, Geczy CL. TLR9 ligands induce S100A8 in macrophages via a STAT3-dependent pathway which requires IL-10 and PGE2. PloS one. 2014; 9:e103629. [PubMed: 25098409]
46. Kortylewski M, Kujawski M, Herrmann A, Yang C, Wang L, Liu Y, et al. Toll-like receptor 9 activation of signal transducer and activator of transcription 3 constrains its agonist-based immunotherapy. Cancer Res. 2009; 69:2497–505. [PubMed: 19258507]

47. Kujawski M, Zhang C, Herrmann A, Reckamp K, Scuto A, Jensen M, et al. Targeting STAT3 in adoptively transferred T cells promotes their in vivo expansion and antitumor effects. Cancer Res. 2010; 70:9599–610. [PubMed: 21118964]

48. Wang L, Yi T, Kortylewski M, Pardoll DM, Zeng D, Yu H. IL-17 can promote tumor growth through an IL-6-Stat3 signaling pathway. J Exp Med. 2009; 206:1457–64. [PubMed: 19564351]

49. Kaech SM, Cui W. Transcriptional control of effector and memory CD8+ T cell differentiation. Nat Rev Immunol. 2012; 12:749–61. [PubMed: 23080391]

50. Maenhout SK, Du Four S, Corthals J, Neyns B, Thielemans K, Aerts JL. AZD1480 delays tumor growth in a melanoma model while enhancing the suppressive activity of myeloid-derived suppressor cells. Oncotarget. 2014; 5:6801–15. [PubMed: 25149535]

TRANSLATIONAL RELEVANCE

Despite the initial efficacy of hormone therapies prostate tumors eventually progress to metastatic castration-resistant prostate cancers (mCRPC), which resist current therapies and also the emerging immunotherapeutic regimens. The advanced prostate cancers develop potently immunosuppressive microenvironment which partly relies on the heterogeneous population of myeloid-derived suppressor cells (MDSCs). We identified a specific population of granulocytic MDSCs that accumulated in patients' circulation during prostate cancer progression from localized to metastatic disease. These $TLR9^{+}$ MDSCs showed high levels of immunosuppressive mediators, STAT3 and Arginase-1, and inhibited effector T cell proliferation and activity. Targeting MDSCs using CpG-*STAT3*siRNA strategy alleviated their immunosuppressive functions restoring T cell activity. With the ongoing clinical translation of CpG-*STAT3*siRNA conjugates to therapy of hematologic malignancies, our results underscore the potential of utilizing these oligonucleotide reagents to immunotherapy of advanced prostate cancers.

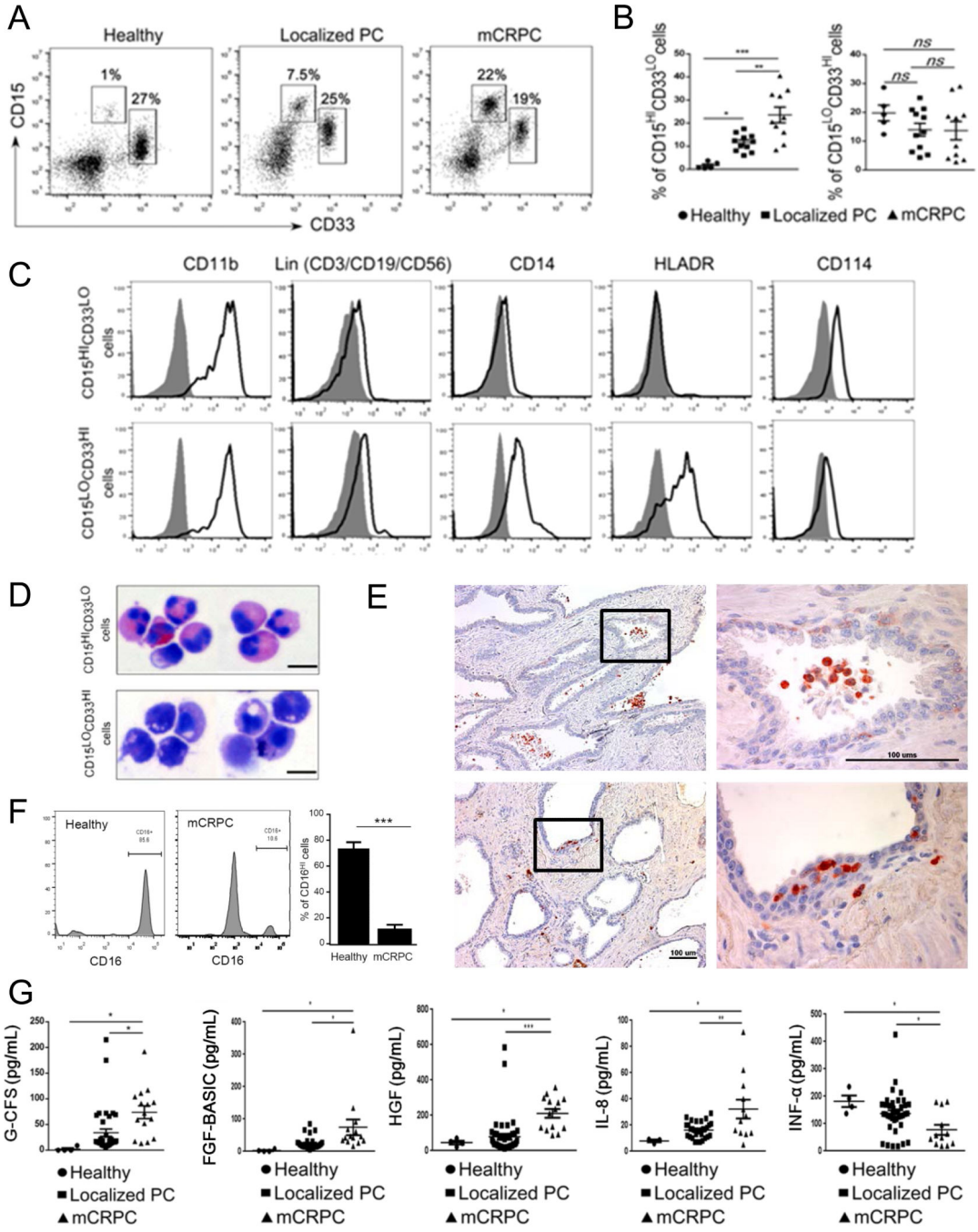

Figure 1. CD15^{HI} myeloid cells accumulate in peripheral blood and tumor tissues in prostate cancer patients with disease progression

(A-B) Flow cytometric analysis of fresh PBMCs from healthy subjects and prostate cancer patients with localized or metastatic disease. Representative dot plots (A) and graphs combining data from all subjects (B) showing percentages of CD15^{HI}CD33^{LO} or CD15^{LO}CD33^{HI} cells in prostate cancer patients' circulation at localized prostate cancers (PC) (n = 11) or metastatic tumors (mCRPC) (n = 10) compared to healthy donors (n = 5). Shown are means ± SD. (C) Representative histograms showing expression of lineage markers (Lin = CD3/CD19/CD56), CD11b, CD14, HLA-DR and CD114 (G-CSFR) among

$CD15^{LO}CD33^{HI}$ (top row) and $CD15^{HI}CD33^{LO}$ (bottom row) cells. (D) Cellular morphology of sorted, cytospinned and stained $CD15^{HI}CD33^{LO}$ or $CD15^{LO}CD33^{HI}$ myeloid cells. Representative microphotographs showing monocytic (top) and granulocytic polymorphonuclear (PMN) phenotype (bottom) of $CD15^{HI}CD33^{LO}$ and $CD15^{LO}CD33^{HI}$ cells, respectively. (E) $CD15^{+}$ cells in cancer patients' prostate tissues have granulocytic and PMN phenotype. Representative results of immunohistochemical staining on FFPE sections from two different patients (top and bottom); scale bar = 100 μm. (F) Mature $CD16^{HI}$ neutrophils are only minor fraction of circulating $CD15^{HI}CD33^{LO}$ cells in prostate cancer patients. The expression of CD16 was assessed on granulocytic cells from healthy subjects or prostate cancer patients. Shown are representative dot plot graphs (two left panels) and the summary of results from six different patients (right bar graph); means ± SD (n = 6). (G) Plasma levels of G-CSF and several other growth factors/chemokines increase with prostate cancer progression in contrast to reduced levels of proinflammatory IFNα. Luminex-based analysis of plasma samples from prostate cancer patients with localized (n = 25) or metastatic tumors (n = 15) compared to healthy individuals (n = 4). Statistically significant differences were indicated by asterisks; means ± SD.

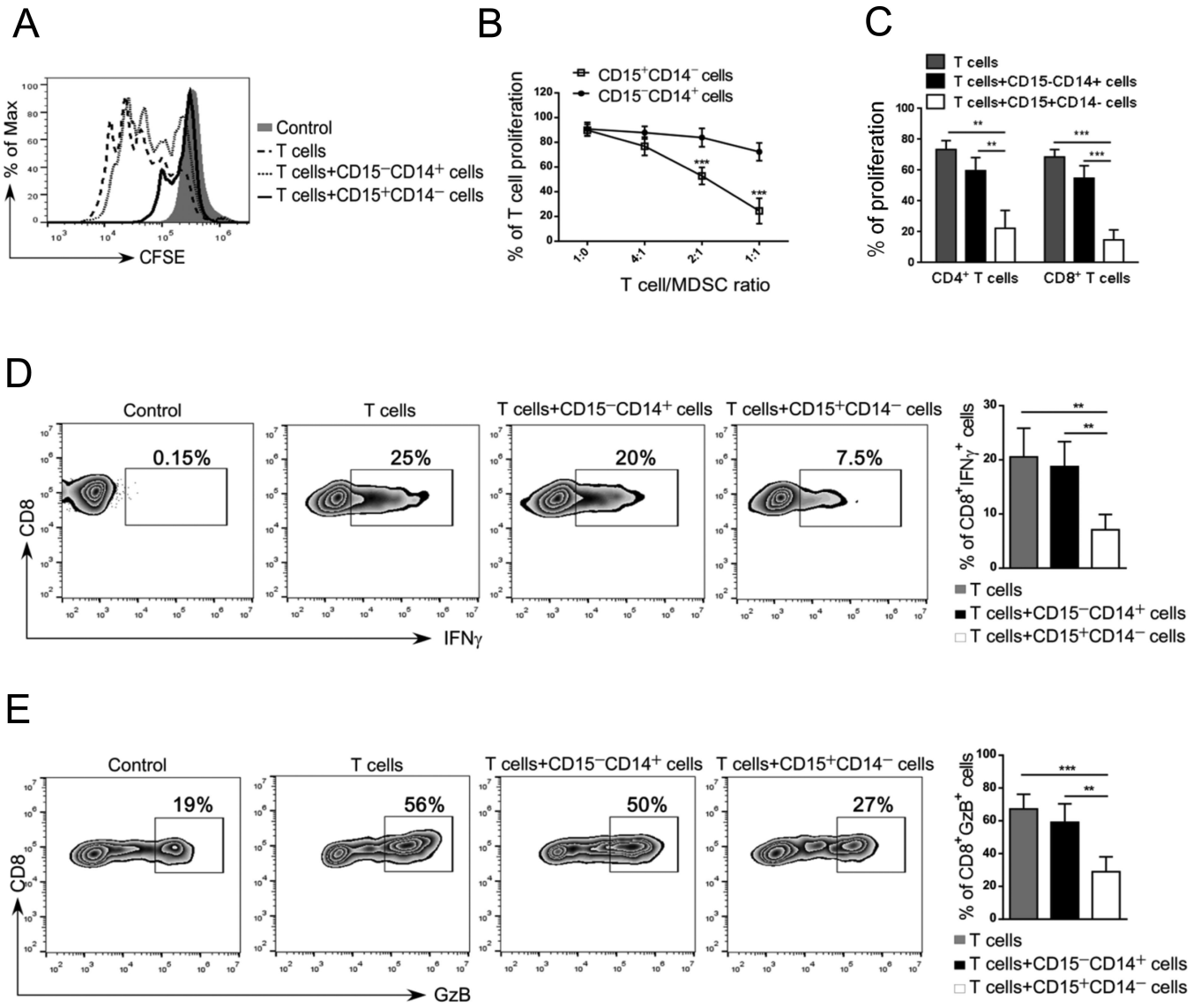

Figure 2. CD15^{HI} MDSCs isolated from prostate cancer patients inhibit proliferation and activity of autologous T cells

(A-C) CD15^{+}CD14^{-} granulocytic and CD15^{-}CD14^{+} monocytic cell populations freshly enriched from metastatic prostate cancer patients' PBMCs were cultured separately with 24 autologous T cells in presence of CD3-/ CD28-specific antibodies for stimulation. (A) Representative flow cytometry data showing T cell proliferation assessed by CFSE dilution after 3 days of co-culture. (B) Combined results of T cell proliferation assays from 5 patients showing percentage of total T cell proliferation at different T: myeloid cell ratios. (C) Proliferation of CD4^{+} and CD8^{+} T cells when incubated at 1:1 ratio with or without the indicated myeloid cell populations; means ± SD (n = 5). (D-E) CD15^{+}CD14^{-} myeloid cells inhibit production of IFNγ and granzyme B by activated CD8^{+} T cells. T cells were co-cultured with either one of myeloid cell populations at 1:1 ratio as above. The intracellular levels of IFNγ and granzyme B were measured using flow cytometry. Representative dot plots and bar graphs showing percentages of CD8^{+}IFNγ^{+} T cells (D) and CD8^{+}Granzyme-

B^+ T cells (E) after 3 days of culture; shown are means ± SD (n = 5). Statistically significant differences were indicated by asterisks.

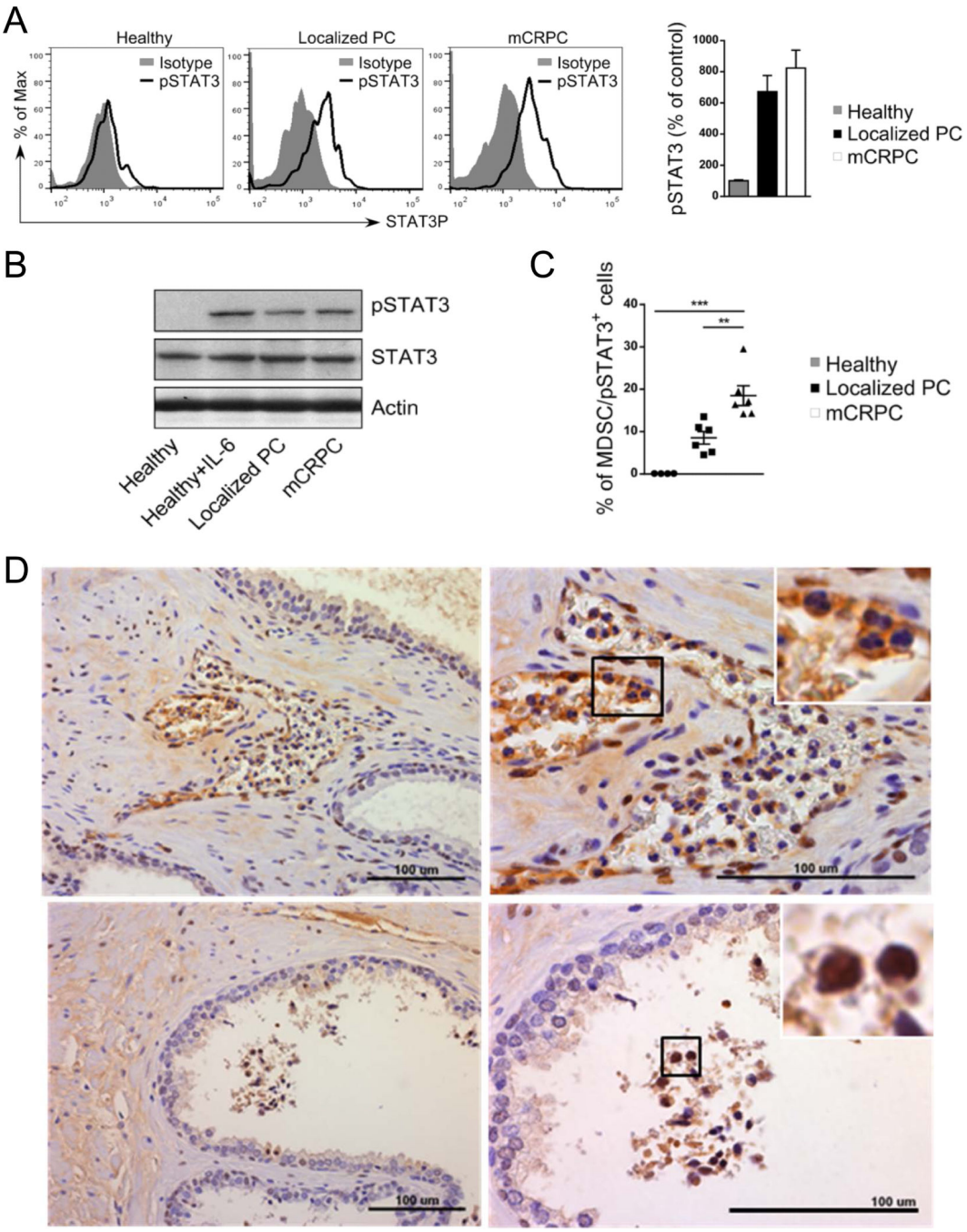

Figure 3. STAT3 activity is elevated in CD15^{HI} MDSCs in prostate cancer patients

(A) Flow cytometric analysis of activated STAT3 (pSTAT3) in granulocytic MDSCs (CD15^{HI}CD33^{LO}) from patients with localized (n = 6) and metastatic (n = 6) prostate cancers compared to granulocytes from healthy individuals (n = 5). Shown are representative histogram overlays and bar graph summary of data from all patients; average of mean fluorescence intensities (MFI) ± SD. (B) Prostate cancer patients' granulocytic cells show increased STAT3 phosphorylation without changes in the total STAT3 protein levels. Western blotting analysis to compare pSTAT3 and total STAT3 protein levels in CD15^{+}

$CD14^{-}$ cells isolated from PBMCs pooled from prostate cancer patients or healthy donors. (C) The percentage of MDSCs ($CD15^{HI}CD33^{LO}$) with activated STAT3 increases with prostate cancer progression. Summary of results from all tested patients; statistically significant differences were indicated by asterisks. (D) Increased infiltration of pSTAT3-positive cells with granulocytic (PMN) morphology in prostate tissues from high-risk prostate cancer patients. FFPE tissue sections were stained using immunohistochemistry for pSTAT3 and analyzed using bright field microscopy. Arrows indicate $pSTAT3^{+}$ PMN cells accumulating within capillaries and venules (top) and involving the glandular lumen (bottom). Shown are representative images from two of ten analyzed specimens; scale bars = 100 μm.

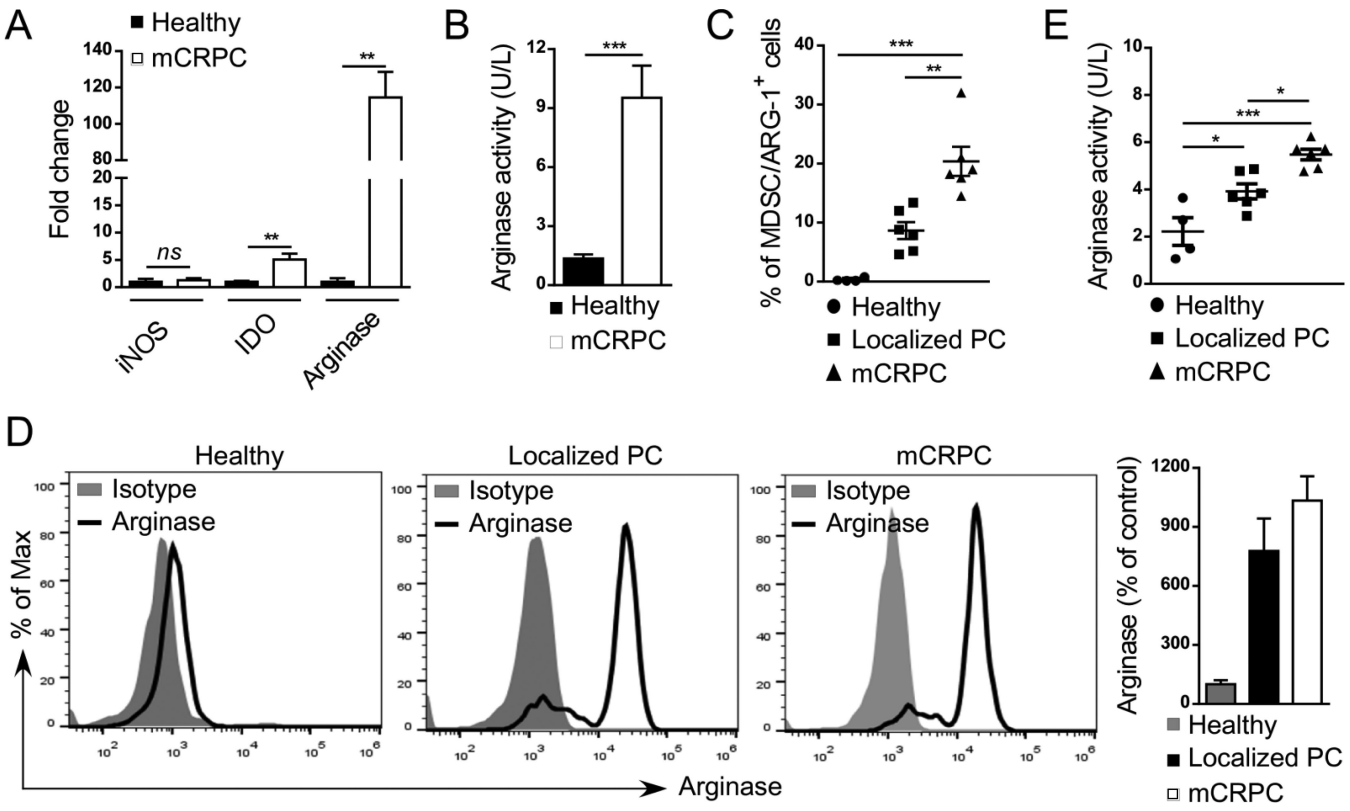

Figure 4. The percentage of arginase-expressing MDSCs increases with prostate cancer progression

(A, B) Arginase 1 expression and activity is highly elevated in G-MDSCs from mCRPC patients. Levels of *ARG1* mRNA in comparison to *IDO* and *iNOS* transcripts (A) as well as intracellular activity of Arginase 1 (B) were assessed in $CD15^{+}CD14^{-}$ G-MDSCs using real-time qPCR and QuantiChrom™ assays, respectively. Shown are means ± SD ($n = 4$). (C) Prostate cancer progression correlates with increase in the percentage of arginase-expressing $CD15^{HI}CD33^{LO}$ G-MDSCs. Flow cytometric analysis comparing PBMCs from healthy individuals ($n = 4$) with prostate cancer patients with localized disease ($n = 6$) or mCRPCs ($n = 6$); means ± SD. (D) High intracellular levels of arginase expression in G-MDSCs from prostate cancer patients compared to granulocytes from healthy subjects as assessed using flow cytometry. Representative histograms (three left panels) and bar graph combining all data (right) from one of three experiments are shown; means ± SD. (E) Plasma levels of arginase activity increase with disease progression as measured in blood samples from in healthy individuals ($n = 4$), prostate cancer patients with localized ($n = 6$) and metastatic disease ($n = 6$); means ± SD. Statistically significant differences were indicated by asterisks.

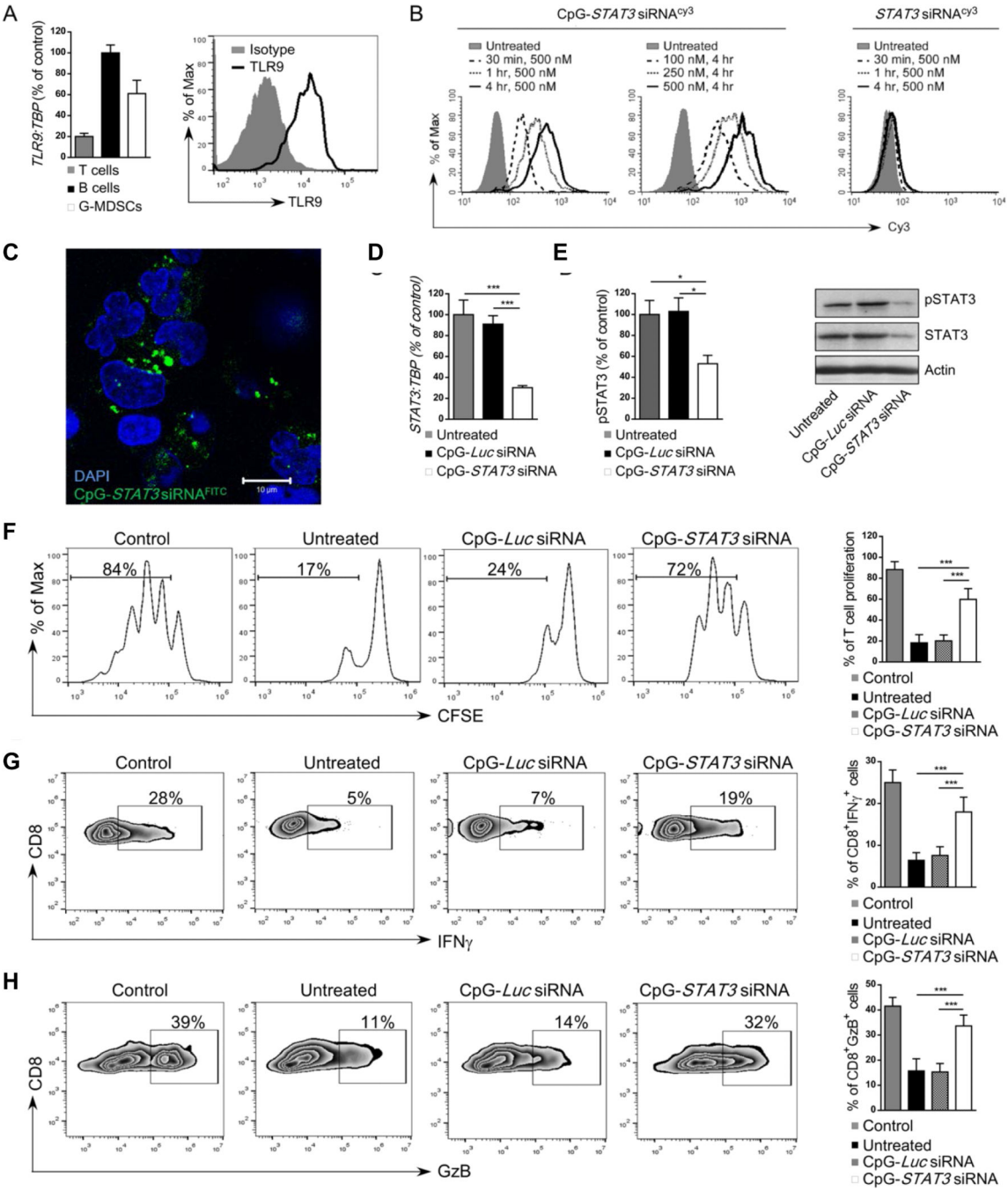

Figure 5. Targeted STAT3 silencing using CpG-*STAT3*siRNA strategy abrogates immunosuppressive activity of granulocytic MDSCs

(A) $CD15^{HI}CD33^{LO}$ G-MDSCs express TLR9 at mRNA or protein levels as assessed by using real-time qPCR (left) or flow cytometry (right), respectively. $CD19^{+}$ B cells and $CD3^{+}$ T cells were used as positive and negative controls for qPCR analysis (left), respectively. (B) Dose- and time-dependent internalization of CpG-*STAT3* siRNA by $CD15^{HI}CD33^{LO}$ MDSCs. PBMCs from prostate cancer patients were incubated with fluorescently-labeled CpG-*STAT3* $siRNA^{Cy3}$ conjugate or unconjugated *STAT3* $siRNA^{Cy3}$ for the indicated times

and doses without any transfection reagents. Percentages of $Cy3^+$ $CD15^{HI}CD33^{LO}$ MDSCs were assessed by flow cytometry; shown are representative results from one of three experiments. (C) *STAT3* siRNA localizes to perinuclear/cytoplasmic cell compartment shortly after internalization. G-MDSCs ($CD15^+CD14^-$) enriched from mCRPC patient were incubated with 500 nM CpG-*STAT3*$siRNA^{FITC}$ for 1 h. The localization of the labeled siRNA part of the conjugate was assessed using confocal microscopy; scale bar = 10 μm. (D-E) CpG-*STAT3* siRNA induces *STAT3* silencing in fresh granulocytic MDSCs. The G-MDSCs enriched from prostate cancer patients' PBMCs were treated with 500 nM CpG-*STAT3* siRNA or CpG-*Luc* siRNA, used a s a negative control, for 48 h. The level of STAT3 inhibition was measured at mRNA level (D) using real time qPCR or at protein level using flow cytometry (E, left) or western blotting (E, right) after staining with antibodies specific to pSTAT3 and/or total STAT3. Statistically significant differences were indicated by asterisks; shown are means ± SD ($n = 5$). (F-H) $CD15^+CD14^-$ MDSCs isolated from prostate cancer patients were treated with CpG-*STAT3* siRNA or control CpG-*Luc* siRNA for 18 h and then co-cultured with autologous $CD3^+$ T cells at 1:1 ratio with anti-CD3/CD28 stimulation. (F) T cell proliferation was determined by CFSE dilution assay after 72 h of co-culture with fresh MDSC. Under same experimental conditions percentages of IFNγ- (G) or Granzyme B- (H) producing $CD8^+$ T cells were assessed using flow cytometry. Shown are representative data from one of two experiments (left four panels) and bar graphs (right panel) combining results from analyses of 5 individual patients' samples; means ± SD. Statistically significant differences were indicated by asterisks.

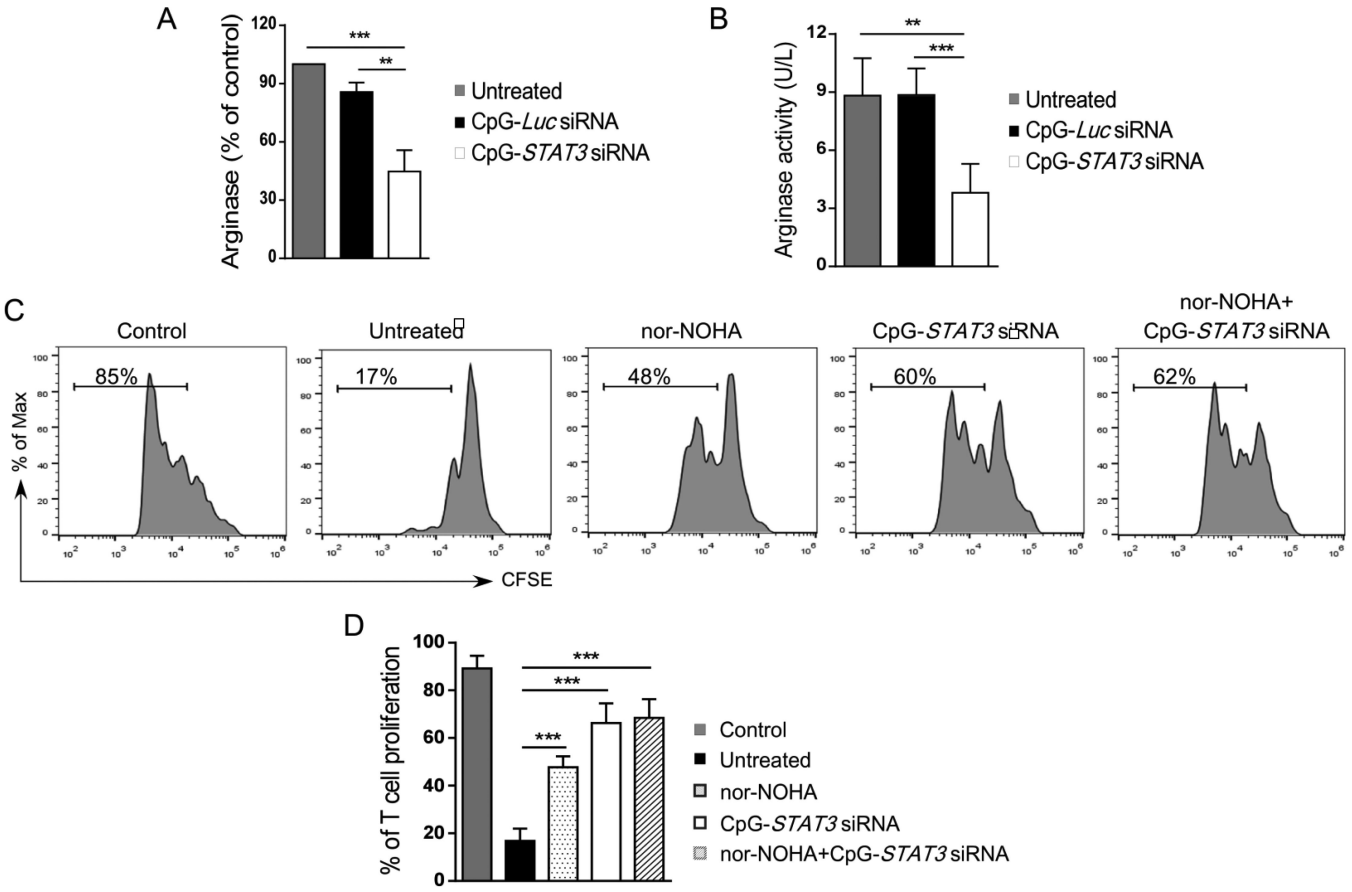

Figure 6. CpG-*STAT3* siRNA blocks arginase expression and inhibits functions of granulocytic MDSCs

(A, B) STAT3 targeting using CpG-siRNA strategy inhibits arginase expression and activity in granulocytic MDSCs. Levels of arginase mRNA (A) and enzymatic activity (B) were assessed in cell lysates using qPCR and QuantiChrom™ assays, respectively, in $CD15^{+}CD14^{-}$ granulocytic MDSCs after 48 h incubation with CpG-*STAT3* siRNA, CpG-*Luc* siRNA or without any treatment. (C, D) Selective STAT3 inhibition alleviates immunosuppressive effect of MDSCs to greater extent than arginase inhibitor (nor-NOHA). Representative data from one of two experiments (C) and the summary of T cell proliferation assays (D) co-cultured in the presence or absence of MDSCs, nor-NOHA (20μM) and the indicated CpG-siRNAs (500 nM). Shown are means ± SD (n = 5). Statistically significant differences were indicated by asterisks.